Available online at www.sciencedirect.com
SCIENCE DIRECT
Catalysis Today 112 (2006) 99–102
CATALYSIS TODAY
www.elsevier.com/locate/cattod

# Oxygen mobility in $LaCoO_3$ perovskites

S. Royer [a], D. Duprez [b], S. Kaliaguine [a,*]

[a] Department of Chemical Engineering, Laval University, Ste Foy, Québec, G1K 7P4 Canada
[b] LACCO–UMR CNRS 6503, Université de Poitiers, F-86022 Poitiers, Cedex, France

Available online 27 December 2005

**Abstract**

This work reports a study of oxygen mobility in a variety of $LaCo_{1-x}Fe_xO_3$ perovskites. The methods used to evaluate oxygen reactivity were temperature programmed oxygen desorption and oxygen isotopic exchange. Three kinds of oxygen are distinguished, depending on their reactivities. First, surface oxygens were found to be the most active forms of oxygen. In oxygen desorption experiments, they are responsible for two desorption peaks, designated as $\alpha_1$- and $\alpha_2$-oxygens in this work. Grain boundary oxygen is distinguished from bulk oxygen, and is proposed to be responsible for β-oxygen desorption observed at high temperature (>750 °C). These two kinds of oxygen, surface and grain boundary oxygen, are however quickly exchanged with the gaseous oxygen during the isotopic exchange reaction. The third kind, and less reactive, oxygen species is proposed to be the bulk oxygen. The mobility of this oxygen in the bulk of $LaCoO_3$ is measured by the initial rate of isotopic exchange. Its mobility is related to the activation of the bulk $Co^{3+}$, and migration of some anionic vacancies.


*Keywords:* Perovskite; Oxygen mobility; Oxygen isotopic exchange; Temperature programmed oxygen desorption

## 1. Introduction

Perovskites are mixed oxides of general formula $ABC_3$ with A and B cations in dodecahedral and octahedral environments, respectively. Since the beginning of the 70's, some oxidic perovskites ($ABO_3$) have been known to be efficient catalysts for gas phase oxidation reactions [1]. Among the possible compositions, cobalt and manganese based perovskites were found to be highly active [2–4]. Nevertheless, the perovskites generally display low specific surface areas [4], depending on the synthesis conditions of the solids. A raise in activity is generally observed with the increase in specific surface area, as discussed by Gunaserakan et al. [5] who tested $La_{0.8}Sr_{0.2}MnO_3$ (prepared by the Pechini method) calcined at different temperatures in the $CH_4$ oxidation reaction. Voorhoeve [6] first distinguished two different oxidation mechanisms, depending on the molecule to oxidize, designated as suprafacial (CO) and intrafacial ($CH_4$) mechanisms. The distinction between the two processes was made on the basis of the type of oxygen involved in the oxidation reaction. For the suprafacial reactions, the reaction between the oxygen dissociatively adsorbed on the surface and the molecule to oxidize is proposed as the rate limiting step. Contrarily, the intrafacial reactions occur when lattice oxygen becomes involved in the reaction. Then, the removal of a lattice oxygen, or the process of reoxidation of the transition metal (and the incorporation of the dissociated oxygen into the bulk), becomes rate determining.

In this work, two methods were used to measure the oxygen mobility in $LaCoO_3$ perovskites synthesized by different routes: temperature programmed oxygen desorption (TPD–$O_2$) and oxygen isotopic exchange (OIE) in order to propose a view of the oxygen mobility in $LaCoO_3$ perovskites.

## 2. Experimental

### 2.1. Sample synthesis

In this work, results obtained in different studies are summarized in order to propose a view of the oxygen mobility in nanocrystalline $LaCoO_3$. Then, $LaCoO_3$ was synthesized by different procedures. The SS sample was synthesized by solid state reaction of the oxide precursors at high temperature (1000 °C) [7]. The COP sample was prepared by simultaneous precipitation of the nitrate precursors [7]. After drying, the solid

* Corresponding author. Tel.: +1 418 656 2708; fax: +1 418 656 3810.
*E-mail address:* serge.kaliaguine@gch.ulaval.ca (S. Kaliaguine).

0920-5861/$ – see front matter © 2005 Published by Elsevier B.V.
doi:10.1016/j.cattod.2005.11.020

was calcined at 700 °C. The CIT sample was synthesized by complexation of the nitrate salts by citric acid [7], followed by calcination of the dried precursor at 600 °C. Different samples were crystallized by grinding of the single oxide precursors. Among these samples, Co1, Co2 and RG were ground under different conditions in order to obtain specific surface areas over a large range. For sample Co1 synthesis, $La_2O_3$ and $Co_3O_4$ as precursors were ground in one-step, resulting in a low specific surface area [8]. Co2 [8] and RG [7] were ground in two-steps. After a first step for perovskite crystallization, an additive (with a mass ratio additive/perovskite equal to 1) was added to the perovskite, and the mixture (additive + perovskite) was ground for a second step for about 20 h. NaCl (Co2) or ZnO (RG) were used as additives for this second grinding step. At the end of this grinding step, the additive was dissolved, and the perovskite obtained was calcined under air (ramp = 2 h, 4 h at 550 °C). Finally, the COPRG sample was synthesized by grinding of an amorphous coprecipitate (obtained following the procedure described for the COP synthesis). The so obtained precipitate was dried and calcined at 500 °C, and then ground in two steps, as for RG.

### 2.2. Characterization

X-ray diffraction patterns were obtained using a SIEMENS D5000 diffractometer with CuKα radiation, for 2$\theta$ between 15 and 75°. Specific surface areas were determined by the BET method from the $N_2$ adsorption isotherms recorded at −196 °C using an OMNISORP 100 instrument. Prior to these measurements, the samples were evacuated at 200 °C for 4 h. Sample compositions were measured by ICP using a P40 apparatus from Perkin-Elmer.

Oxygen thermodesorption (TPD–$O_2$) were performed on a RMX100 multi catalyst testing system (Advanced Scientific Desing Inc.) equipped with a quadrupolar mass spectrometer and a TCD for analysis. Conditions of test were: 10 NmL/min He, T from 25 to 900 °C with a ramp of 5 °C/min. Before the desorption experiments, the samples were calcined at their respective calcination temperature under 20% $O_2$ in He (20 mL/min).

Oxygen exchange experiments were carried out in a recycle U-shaped microreactor coupled to a quadrupolar mass spectrometer. A pressure of 50 mbar of $^{18}O_2$ was set in the reactor at the temperature of test, and evolutions of $^{18}O_2$, $^{16}O_2$ and $^{18}O^{16}O$ concentrations recorded on the MS. Before test, samples were calcined at their calcination temperatures under $O_2$.

More detailed information about the experimental procedures and apparatus can be found in the above cited references [7–10].

## 3. Results and discussion

### 3.1. Physical properties

All the synthesis procedures result in the perovskite phase crystallization (JCPDS card 09–0358) (Table 1). Weak reflexions attributed to $Co_3O_4$ (JCPDS card 42–1467) were also observed for SS, Co1 and COPRG. As observed from Table 1, synthesis conditions, and especially calcination temperatures were found to strongly affect the specific surface area of the solids. Crystal growth and agglomeration processes can explain the observed decrease in specific surface area as the calcination temperature is raised. Then, the higher the calcination temperature, the higher the crystal domain size ($D_1$ in Table 1), and the lower the specific surface area ($S_{BET}$ in Table 1). It is however observed that a fraction of the surface area is generally lost by contact between the elementary crystals. This is characterized by the $S_{th}/S_{BET}$ ratio (see Table 1), which varies over a large range (from 27.8 for SS to 2.2 for COPRG), and is explained by the occurrence of grain boundaries between crystals. Then, the higher the calcination temperature, the higher the crystal domain size, and also the higher the $S_{th}/S_{BET}$ ratio.

### 3.2. Oxygen mobility in $LaCoO_3$

#### 3.2.1. Temperature programmed oxygen desorption

The TPD experiments revealed the desorption of three kinds of oxygen which were designated as $\alpha_1$, $\alpha_2$ and β as mentioned above [7]. The global amount of oxygen desorbed as $\alpha_1$- and

Table 1
Physical properties of the samples

| Sample | SS | COP | CIT | RG | Co1 | Co2 | COPRG |
|---|---|---|---|---|---|---|---|
| Ref. | [7] | [7] | [7] | [8] | [8] | [8] | [7] |
| Calcin. temp. (°C) | 1000 | 700 | 600 | 550 | 550 | 550 | 550 |
| Formula[a] | $LaCo_{0.97}O_3$ | $LaCo_{0.98}O_3$ | $LaCo_{0.96}O_3$ | $LaCo_{0.80}Fe_{0.20}O_3$ | $La_{0.94}Co_{0.97}Fe_{0.03}O_3$ | $La_{0.93}Co_{0.90}Fe_{0.10}O_3$ | $LaCo_{0.93}Fe_{0.03}O_3$ |
| Crystalline phases[b] | P, weak Co | P | P | P | P, weak Co | P | P, weak Co |
| $D_1$ (nm)[c] | 73.9 | 32.2 | 26.9 | 16.3 | 16.4 | 16.4 | 16.5 |
| $S_{BET}$ ($m^2\,g^{-1}$)[d] | 0.4 | 3.5 | 6.6 | 17.1 | 4.2 | 10.9 | 18.7 |
| $S_{th}/S_{BET}$[e] | 27.8 | 7.3 | 4.6 | 2.9 | 11.9 | 4.6 | 2.2 |

(f) Calcined at 200 °C, (g) respectively calcined at 200–300–500 °C.
[a] Measured by ICP.
[b] Phase recognition by comparison with JCPDS files (P, perovskite; C, $Co_3O_4$).
[c] Crystal domain size evaluated by mean of the Scherrer equation after Warren's correction for instrumental broadening.
[d] Calculated by the BET method from $N_2$ adsorption isotherms.
[e] Ratio between the theoretical surface area and the BET surface area. Theoretical surface area evaluated supposing cubic particle shape of size $D_1$ and crystal density of 7.29.

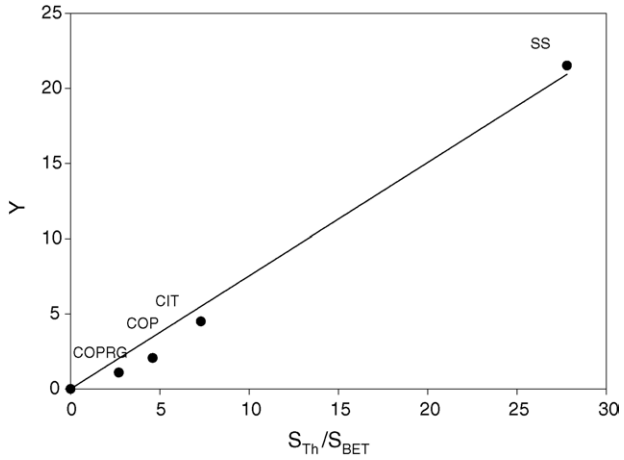


Fig. 1. Evolution of $Y$ as a function of the ratio $S_{Th}/S_{BET}$ (one monolayer was assumed to correspond to 4 μmol $m^{-2}$). $Y$: number of monolayers desorbed.

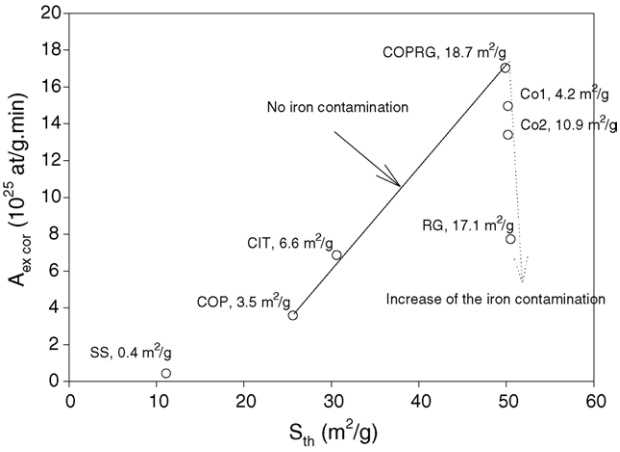


Fig. 2. Corrected pre-exponential factor obtained for the oxygen isotopic exchange on a variety of $LaCo_{1-x}Fe_xO_3$ as a function the theoretical surface area [8].

$\alpha_2$-was found to be essentially proportional to the BET surface area, suggesting for these two desorption processes that the oxygen is evolving from the solid surface. Most of the adsorbed oxygen is in the form of a $O_2^-$ ion radical having an excess of electronic charge (as evidenced by XPS in [8]). The temperatures of desorption, observed for $\alpha_1$- and $\alpha_2$-oxygen, suggest that $O_2^-$ can be found on sites giving rise to different heats of adsorption. The possible presence of neighbor sites ($Co^{3+}O^-$, as suggested in [7]) could interact with the oxygen adsorbed on the low coordination cobalt sites ($Co^{3+}O_2^-$), and facilitate the desorption process ($\alpha_1$-desorption process). Desorption from isolated $Co^{3+}O_2^-$ occurs logically at higher temperature ($\alpha_2$-desorption process). Finally, because of the relationship observed in Fig. 1 between the $S_{th}/S_{BET}$ ratio and the number of monolayers desorbed as β-oxygen, it was proposed that β-oxygen desorbed from the reduction of some $Co^{3+}$ located in the grain boundaries of the solids. This graph indeed suggests that the number of oxygen monolayers per unit theoretical surface area ($S_{th}$) is essentially constant. The transfer of oxygen ions would then essentially occur within the grain boundaries. This mechanism supposes higher rates of oxygen diffusion in the grain boundaries than in the bulk. Bulk cobalt is not activated up to 900 °C, and then no bulk oxygen mobility (or bulk $Co^{3+}$ reduction) is observed by TPD.

### 3.2.2. Oxygen isotopic exchange reaction (OIE)

Results obtained with $LaCoO_3$ suggest that the simple heteroexchange is the main mechanism of exchange on the $LaCoO_3$ samples. It cannot however be excluded that some complex heteroexchange also occurs on $LaCoO_3$ samples. Moreover, it was observed that all the oxygen atoms of the crystal are able of exchange with gaseous oxygen.

It is observed that exchange activity, as measured by the initial rate of exchange [10], is not correlated with the specific surface area of the sample. A better relation can be obtained between the exchange activity and the theoretical surface area (Fig. 2). Then, the larger the crystal domain size (and thus the higher the $S_{th}$), the higher the exchange activity. It can be observed on this figure that iron contamination induces a decrease of the oxygen mobility in the crystal (compare Fig. 2, dotted lines with samples composition in Table 1).

### 3.3. Mechanism of oxygen mobility

Results obtained by temperature programmed oxygen desorption and oxygen isotopic exchange allowed to distinguish three kinds of oxygen, which present different reactivities (or mobilities) depending on their location in the solid. Oxygen reactivity varies as follows: surface oxygen > grain boundary oxygen > bulk oxygen.

Surface lattice oxygen can be in the form of $O^-$ or $O^{2-}$, as evidenced by XPS by many authors [9,11,12], whereas bulk oxygen is known to be $O^{2-}$ ionic species. The occurrence of some $O_2^-$ superoxide species on the surface of $LaCoO_3$, as proposed for the α-oxygen desorption process and evidenced by XPS in [8], should not be excluded. Grain boundary oxygen species are supposed to be $O^{2-}$ species, since these boundaries are formed by incompatibility between two neighbor crystallographic planes.

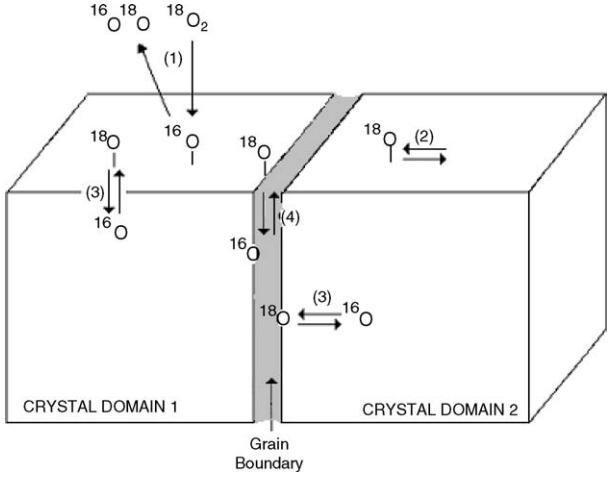


Fig. 3. Scheme of the oxygen mobility in $LaCoO_3$ solids [8].

Oxygen exchange can then be described in terms of elementary steps. First, surface oxygen (represented by $^{16}O$ in Fig. 3 step 1) can react with an adsorbed $O_2$ molecule (exchange reaction) or desorb ($\alpha_1$-and $\alpha_2$-oxygen desorption process), by a mechanism supposing a change in the oxidation state of the cobalt surface atoms (temperature programmed reduction and oxygen storage capacity experiments show an activity of the $Co^{3+}/Co^{2+}$ couple in $LaCoO_3$ at a temperature lower than 200 °C [7,13]). Then, the surface is proposed to be quickly exchanged with gaseous oxygen, after adsorption of a dioxygen molecule on a surface cobalt site ($Co^{2+}$) having an excess of electronic charge (Mars–Van–Krevelen mechanism). The surface oxygen exchanged, after diffusion on the surface (step 2 in Fig. 3), can then exchange with grain boundary oxygen, via a mechanism involving oxygen vacancies: Grain boundaries oxygen is supposed to be more mobile than bulk oxygen. $O^{2-}$ species located in the grain boundaries are also proposed to desorb at high temperature during the TPD experiments ($\beta$–$O_2$). Finally, a bulk oxygen diffusion to the surface (step 3) or to the grain boundaries (step 3′) can occur with similar rates. Thermal reduction of bulk $Co^{3+}$ is however supposed to proceed at a too high temperature under inert atmosphere (>900 °C) for the desorption of bulk oxygen species to be observed by TPD. Following similar considerations, the decrease in oxygen mobility observed with the increase of iron contamination (Fig. 2) can be explained by the low reducibility of iron when located in a perovskite structure [14]. This is in line with the observations made by Nitadori and Misono [15] who reported a low activity in exchange for $LaFeO_3$. Logically, the Co substitution by Fe results in a decrease of the bulk oxygen mobility.

Then, diffusional regimes distinguished by OIE are: surface and grain boundary diffusion ≫ bulk diffusion; whereas only surface diffusion and grain boundary diffusion are discriminated by oxygen thermodesorption.

## 4. Conclusion

The study of the oxygen mobility by two complementary methods allowed to obtain a clear view of the oxygen mobility in the $LaCoO_3$ perovskite crystal. Two kinds of surface oxygen are distinguished by TPD, desorbing at low ($\alpha_1$-$O_2$) and intermediate ($\alpha_2$-$O_2$) temperature. The oxygen desorbing at high temperature ($\beta$-$O_2$) during the TPD experiment was attributed to the reduction of some $Co^{3+}$ located in the grain boundaries of the solid. Bulk oxygen reactivity was however evaluated by mean of the oxygen isotopic exchange reaction. Differences in bulk oxygen mobility, depending on the crystal domain size and degree of iron contamination, were observed for a variety of cobalt based samples.

## References

[1] W.F. Libby, Science 171 (1971) 499.
[2] G. Kremenic, J.M.L. Nieto, J.M.D. Tascon, L.G. Tejuca, J. Chem. Soc. Faraday Trans. 1 (81) (1985) 939.
[3] T. Nitadori, T. Ichiki, M. Misono, Bull. Chem. Soc. Jpn. 61 (1988) 621.
[4] L. Wan, in: L.G. Tejuca, J.L.G. Fierro (Eds.), Properties and Applications of Perovskite-Type Oxides, Marcel Dekker, New York, 1993.
[5] N. Gunasekaran, S. Saddawi, J.J. Carberry, J. Catal. 159 (1996) 107.
[6] R.J.H. Voorhoeve, in: J.J. Burton, R.L. Garten (Eds.), Advances Material in Catalysis, Academic Press, New York, 1977, p. 129.
[7] S. Royer, F. Bérubé, S. Kaliaguine, Appl. Catal A 282 (2005) 273.
[8] S. Royer, A. Van Neste, R. Davidson, S. McIntyre, S. Kaliaguine, Ind. Eng. Chem. Res. 43 (2004) 5670.
[9] S. Kaliaguine, A. Van Neste, V. Szabo, J.E. Gallot, M. Bassir, R. Muzychuk, Appl. Catal. A 209 (2001) 345.
[10] S. Royer, D. Duprez, S. Kaliaguine, J. Catal. 234 (2005) 364.
[11] L.G. Tejuca, J.L.G. Fierro, J.M.D. Tascon, Adv. Catal. 36 (1989) 237.
[12] J. Choisnet, N. Abadzhieva, P. Stefanov, D. Klissurski, J. Chem. Soc. Faraday Trans. 90 (1994) 1987.
[13] S. Royer, H. Alamdari, D. Duprez, S. Kaliaguine, Appl. Catal. B 58 (2005) 275.
[14] P.E. Marti, A. Baiker, Catal. Lett. 26 (1994) 71.
[15] T. Nitadori, M. Misono, J. Catal. 93 (1985) 459.